Advanced Welded Materials Analysis

Evelyn B. Welles, Axel R. Koenig
Institute für Materialwissenschaft, Berlin, Germany

***Abstract*—**The dissimilar joint between aluminium/titanium alloys (Al 6082 and Ti G2) were successfully achieved by CO_2 laser welding with a single pass and without filler material using the overlap joint design. Laser welding parameters ranges combinations were experimentally determined using Taguchi approach with the objective of producing welded joint with acceptable welding profile and high quality of mechanical properties. In this study a joining of dissimilar Al 6082 / Ti G2 resulted in three distinct regions fusion area in the weldment. These regions are studied in terms of its microstructural characteristics and microhardness which are directly affecting the welding quality.

The weld metal was mainly composed of martensite alpha prime. In two different metals in the two different sides of joint HAZ, grain growth was detected. The microhardness of the joint distribution also has shown microhardness increasing in the HAZ of two base metals and a varying microhardness in fusion zone.

***Keywords*—**Micro-hardness, Microstructure, laser welding, dissimilar jointed materials

I. Introduction

WELDING process is resulting in three distinct regions in the weldment. These are the fusion area (FA), also known as the weld metal, the heat-affected zone (HAZ), and the unaffected base metal (BM). The FA experiences melting and solidification, and its microstructural characteristics are directly affecting the welding quality. The microstructure growth in the FA depends on the solidification behaviour of the weld pool. The principles of solidification control the size and shape of the grains, segregation, and the distribution of inclusions and porosity. Solidification is also critical to the hot-cracking behaviour of alloys. FA can be considered as mini-casting region. Therefore, parameters important in determining microstructures in casting, such as growth rate, temperature gradient, under cooling, and alloy composition determine the development of microstructures in welds as well. But unlike in casting, during welding, where the molten pool is moved through the material, the growth rate and temperature gradient vary considerably across the weld pool. In welds, weld pool solidification often occurs without a nucleation barrier. Therefore, no significant under-cooling of the liquid is required for nucleation of the solid. Solidification occurs instinctively by epitaxial growth (the growth of one layer of crystals on another such that they have the same structure) on the partially melted grains during autogenous welding. Generally, weld solidification models assume epitaxial growth and for most of the cases the assumption seems to be appropriate. The heat, fluid-flow models and modelling techniques now available can help describe the phase evolution during weld solidification.

A microstructure of the 3D parts, built by rapid prototyping (RP) based on deposition by GTA welding was examined by [1]. Material used for building 3D parts was AISI 1018. The microstructure analysis of fusion and the heat-affected zone was performed. Different heat-transfer conditions cause different cooling rates and, consequently, different microstructures. Thus, all the deposited beads exhibit equiaxed dendrites at the top layer, but different grain sizes within the bead with different conditions. The best microstructure was achieved with samples that have the most uniform heat-transfer conditions at 360º angle. Samples were examined on Vickers micro-hardness tests. The results from all samples showed that layers possess a maximum microhardness at the top deposited layer, while there was a slight decreasing trend towards the middle and the bottom layers. The obtained results show that RP based on GTA welding can be successfully used for building 3D parts. To further improve the quality of deposited layers, it is necessary to adjust the heat input according to the volume of the heat sink, so that the same maximum temperature was achieved across the layers. Caiazzo et al. [2] have an experimental study carried out on Ti6Al4V using CO_2 laser welding about both the weld bead geometry and mechanical properties. Two different shielding gases (He and Ar) were used and the results obtained illustrated the different behaviours of the welded material both qualitatively (i.e. greater internal defectiveness for Ar) and quantitatively (i.e. greater melting depth for He than for Ar when the welding parameters are equal). Comparison of the geometry weld bead measurement trends highlighted that there is no great difference in these results compared to those obtained using other materials. The micro-hardness values found on the weld bead cross-section underlined a considerable increase, i.e. from 28 to 48%, beginning at the base metal up to the weld pool. These proportional values were approximately twice those of the micro-hardness increase from the base metal up to HAZ. As regards the parameters and thicknesses used, a low welding speed influence on the mean micro-hardness of the joint was noted, caused by the low thermal conductivity of the alloy. The results obtained for the different thicknesses almost emphasized failure that began at the bead foot and spread towards the same bead, HAZ or base metal. Li and Fontana [3] have adopted a laser-welding technique for the fabrication of the hydraulic valves, in which the butt welds joining the AISI304L to the AISI12L13 were performed in such a way as to control solidification cracking and micro-fissuring. Metallurgical analyses revealed that both solidification cracking in the fusion zone and micro-fissuring in the heat affected zone result from S, Pb and P contained in the AISI12L13. The relationships between the redistribution of elements in the fusion

zone, the welding parameters, and the microstructures were investigated. A 0.12 mm off-set of the laser beam towards the AISI304L and an impingement angle of 15° with respect to the fit-up face of the butt joints can produce sound welds on the hydraulic valves made of 0.9 mm thick AISI304L and AISI12L13. E. M. Anawa et al. [7] have an experimental study on tensile shear strength of dissimilar Al/Ti joint which was evaluated as a response function of the selected laser welding factors and statistical model was developed to describe it. The result indicates that the developed model can predict the responses acceptably. Tensile strength of the joints was found to be same as Al base metal. Also the microstructure and microhardness of the joint have been studied.

Zhang et al. [4] have explored a new modelling approach for aluminium weldments. In the approach, the microstructure data calculated from welding analysis are directly transferred to the deformation and damage analysis. With an interpolation equation between the properties of the base metal and the fully reverted HAZ, the exact dimension and gradient of mechanical properties of the whole HAZ are automatically predicted. The overall effect of the microstructure evolution during welding, and the resulting deformation and damage capacity of the welded joint can then be analyzed. Evolution of the microstructure in AISI 1005 steel weldments was studied during GTA welding experimentally and theoretically by [5]. The experimental work involved real-time mapping of phases in the HAZ using a synchrotron-based spatially resolved X-ray diffraction (SRXRD) technique and post weld microstructural characterization of the fusion zone (FZ). A three-dimensional heat transfer and fluid flow model was used to calculate the temperature and velocity fields, thermal cycles, and the geometry of the FZ and the HAZ. The experimental SRXRD phase map and the computed thermal cycles were used to determine the kinetic parameters in the Johnson–Mehl–Avrami (JMA) equation for the ferrite to austenite transformation during heating in the HAZ. The results indicate significant promise for understanding microstructure evolution during GTA welding of AISI 1005 steel by a combination of real time phase mapping and modelling. A one-dimensional numerical diffusion model has been developed by [6] to simulate the kinetics of the austenite (γ) to ferrite (δ) transformation in 2205 duplex stainless steel during welding. In the model, it was assumed that the transformation is driven by the diffusion of nitrogen under Para-equilibrium conditions. Transformation kinetics from both uniform and non-uniform starting microstructures was investigated. Karimzadeh et al. [8] have studied the effect of epitaxial growth on microstructure of Ti– 6Al–4V alloy weldment using an artificial neural network (ANN). The microplasma arc welding (MPAW) procedure was performed at different currents, welding speeds and flow rates of shielding and plasma gas. Microstructural characterizations were studied by optical and scanning electron microscopy (SEM). An artificial neural network was developed to predict grain size of FZ at different currents and welding speeds. The results showed that a coarse primary β phase develops in the fusion zone as a result of epitaxial nucleation on coarsened β grains near the heat affected zone (NHAZ) which grow competitively into the molten weld pool. A combined modelling approach based on the Kampmann and Wagner method was applied by [9], [10] to predict the behaviour of high strength 7xxx aluminium alloys. Thermal modelling, microstructure modelling and strength modelling were performed in succession to give some insight into the complex precipitation mechanism occurring during FSW. An optimized model calibration procedure was also presented for the 7449 alloy. The predicted microstructures are found to be in good quantitative agreement with the characterized experimental microstructures. Predicted precipitate distributions were used to estimate the strength of the material. These predictions generally agreed well with measured hardness values.

II. Experimental Work

A. Materials Specifications

The materials selected to be joined by CO_2 laser welding and subjected to this study are as following: Aluminum 6082 T6 with dimension of 160 x 80 x 2 mm and titanium grade 2 with dimension of 160 x 80 x 1 mm. The chemical composition, mechanical and physical properties of materials selected are exhibited in Tables I-IV.

TABLE I
Chemical Composition of the Al Grades (WT %)

Material	Si	Fe	Mn	Mg	Cr	Zn	Ni	Al
Al 6082	1.05	0.5	0.93	1.05	0.26	0.22	0.008	Bal.

TABLE II
Chemical Composition of the Tigrade 2 (Wt %)

Material	C	Fe	H	N	O	Ti
Ti G2	0.1	0.3	0.015	0.03	0.25	99.2

TABLE III
Mechanical Properties of the Materials

Grade	Tensile Strength, [MPa]	Yield Strength [MPa]	Elongation %	Hardness Brinell [HB], max	Elastic Modulus [GPa]
Al 6082					
Ti G2				14.5	

TABLE IV
Physical Properties of the Materials

Grad	Thermal Conductivity W/m. °C	Melting Point °C	Thermal Expansion µm/m/°C	Density Kg/m3
Al 6082				
Ti G2	16.4		9.36	

B. Description and Use of the Studied Materials

Aluminum, EN AW-6082 is a construction material with good ductility, polishing ability and corrosion resistance, good electrolytic oxidation, suitable for welding. It has good plasticity qualities in an annealed state suitable when hardened. Formability is very good in the temperature range 450 to 500°C. Very good corrosion resistance, this material is not inclined to stress corrosion cracking. Typical product applications include: airplane cabins, helicopter cockpits, floor coverings, door frames,

safety barriers, escalators, furniture, rivet stems, cranes and columns.

The combination of high strength-to-weight ratio, excellent mechanical properties, and corrosion resistance including in Titanium, makes it the best material choice for many critical applications. Titanium grade 2 is used for demanding applications, such as, static and rotating gas turbine engine components. Some of the most critical and highly-stressed civilian and military airframe parts are made of titanium. The use of titanium has expanded in recent years to include applications in nuclear power plants, food processing plants, oil refinery heat exchangers, marine components and medical prostheses.

The high cost of titanium alloy components may limit their use, lower-cost alloys, such as, aluminium and stainless steels, are often chosen instead.

C. Sample Preparation

A dissimilar heterogeneous lap joint between two plates of Al 6082 and Ti G2, of dimensions (160 x 80 x 2 and 160 x 80 x 1) mm respectively, was made using the single pass laser welding process. The titanium plate was the upper plate and exposed to the laser beam to avoid the high reflectivity of aluminium. The welding experiments were carried out following the Taguchi designed matrix (L16) in random order generated by Design Expert software, as presented in Table V. A small sample was cut from selected welded plates (exp. No. 1, 4, 14, and 15) perpendicular to the welding line to study the microstructure and microhardness. Polishing for ferrous materials was carried out using diamond suspensions with grain size of (6, 3 and 0.05 µm). Keller's reagent (1% HF, 1.5% HCl, 2.5% HNO_3 and H_2O solution) was used as etchant for aluminium alloys of dissimilar joints and Reagent consisting of (10 ml HF and 5 ml HNO_3 in 85 ml of water) was used for etchant titanium parts of dissimilar joints.

TABLE V
WELDING INPUT VARIABLES, EXPERIMENT DESIGN LEVELS

Exp. No.	Run	Power, kW	Speed, mm/min	Focus, mm
		1.200		-0.67
		0.675		-1.00
		1.200		-0.33
		0.675		0.00

D. Microstructure

The microstructures of dissimilar joints were inspected by means of optical microscopy coupled with a video camera, exhibited in Fig. 1. The microscopy lenses used for this study were a magnification of 16X for the eye-piece lens and 80X for objective.

E. Microhardness

The Vickers Microhardness tests were measured by means of PMT-3 Microhardness tester at room temperature, exhibited in Fig. 2. A load of 100g was applied for fifteen minutes then the dimensions of the indentation were measured by means of the connected to the same microhardness test. An average of five measured readings were calculated for each location of weld transverse sample (base metal, HAZ and weld pool) and tabulated for further studies. The Vickers hardness number calculation is based on:

$$HV = 1.8544 \times \frac{p}{d_2} \quad (1)$$

where: p = load in Kgf , d = indentation in mm

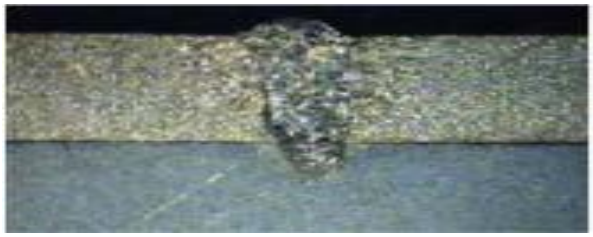

Fig. 1 Lap joint between Al 6082 and Ti G2

Fig. 2 Photograph of Microhardness tester

III. MICROSTRUCTURE OF DISSIMILAR MATERIALS

The specimens prepared of Al6082 / Ti G2 were used for microhardness and microstructure studies. Different grain textures can be clearly observed in Figs. 3 (a)-(d) between the upper WZ and the lower WZ due to the diversity of heat transfer direction. When welding was started before penetration, the heat transferred along cross-direction and depth direction, consequently generated the columnar grains whose orientation was perpendicular to the boundary between the fusion zone and the HAZ in titanium plate as it exhibited in Figs. 3 (b), (c). The input heat mostly transferred along the cross-direction, and thus generated coarse equiaxed grains. No obvious second phase was observed in the WZ at upper part of welding pool and just the solidification crystals were apparent. The microstructure feature is mainly caused by the different weld thermal cycles at two different zones. The optical microscopy micrograph exhibited in Fig. 3 (c) shows that the HAZ in the vicinity of molten boundary of titanium consists of mainly ά martensite. The cooling rate which is estimated to be 10^{4}°C/s [4] is responsible for the martensite structure formation. The martensitic structure in WZ and HAZ is the main reason for improving the tensile strength of the welded titanium components. The circular ά in the HAZ was attributed to rapid cooling of the weld metal. The grain size of the β matrix has been increased greatly by the thermal cycle of the welding as it exhibited in Fig. 3 (d). The laser Al 6082 / Ti G2

dissimilar joining resulted in a complex and heterogeneous microstructure composed of columnar grains and "white solute bands" in the base of welding pool. The liquation zones, evident in aluminium partially melted zones are due to the presence of low fusion point elements (magnesium) at the grain boundaries. Also, it was noted that the reduction in porosity that may be attributed to the following two main reasons:

1. Increased average power (and hence power density) at the specimen. The increased power density at the specimen maintained the stable keyhole during the welding process. The keyhole stayed open during the welding, and the solidification time was increased, allowing the pores to escape on both sides of the seam.
2. Improved gas shielding system design with a coaxial argon shield on the top and bottom of the welded specimen.

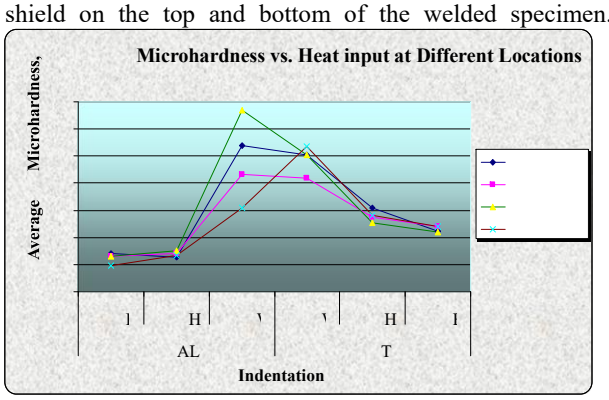

IV. Microhardness of Dissimilar Materials

The specimens selected for microhardness studies were based on heat input calculation (P x S). Vickers microhardness measurements with a 50 g loading force test were applied to the selected specimens shown in Fig 1. For each specimen, three different positions were subjected to the study (BM, HAZ, and WZ) for each side of the dissimilar joint as presented in Table VI and exhibited in microhardness profile of the dissimilar joint Fig. 4. The data on the liquid titanium to liquid aluminum interaction during high solidification rate key-hole laser welding is very limited. In the HAZ of the titanium side, there was an increase in the microhardness (255 – 309 Hv) and a dramatic increase in WZ up to (418- 509 Hv) as presented in Table VI. This could be related to the quenching effect resulting in a martensitic ά microstructure.

TABLE VI
Microhardness Test Result of Dissimilar Ferrous to Nonferrous Materials

Sp No.	Al 6082			Ti G2		
	BM	HAZ	WZ	WZ	HAZ	BM
	139. 5	126.1	537.4		309.3	224.3
	129.6	139.7	430.7	418.1	273.4	241.8
	131.4	150.2	669.4	504.3	255.6	219.9
	96.6	135.4	308.8	536.0	280. 8	241.6

Compared to the hardening effect observed in the weld–aluminium interfaces by intermetallic compound generation, the titanium–weld interfaces were not expected to be the weakest point of the assemblies. The fractures mostly occurred at the aluminium WZ and referring to the microhardness result measured and presented in Table VI and Fig. 4 presents the microhardness profile the aluminium WZ (up to 670 HV). The fracture could be interpreted as being due to a loss in the ductility of aluminium and due to the brittle components formed during solidification stage in WZ at aluminium side.

Compared to the hardening effect evident in the weld–aluminium interfaces by intermetallic compound generation, the titanium–weld interfaces were not expected to be the weakest point of the assemblies. The fracture was mostly occurring at the aluminium WZ and referring to the microstructure transformation during the welding process which is evident from the microhardness result measured and presented in Table VI and Fig 4 microhardness profile. The fracture could be interpreted by losing the ductility of aluminium and due to the brittle components formed during the solidification stage in WZ at aluminium side.

V. Conclusion

- The dissimilar joint between aluminium alloys (Al 6082 and Ti G2) alloys were successfully welded by CO_2 laser welding with a single pass and without filler material using the overlap joint design.
- The weld metal was mainly composed of martensite alpha prime. In two different metals in the two different joints HAZ, grain growth was detected.
- The microhardness of the joint distribution also has shown microhardness increasing in the HAZ of two base metals and a varying microhardness in fusion zone.

- CO_2 laser welding which is characterized by low heat input for joint dissimilar components which have different thermal conductivity and different thermal expansion may not affect the welding quality.

REFERENCES

[1] Z. Jandric, M. Labudovic and R. Kovacevic, Effect of heat sink on microstructure of three-dimensional parts built by welding-based deposition, International J. of Machine Tools and Manufacture, Vol. 44, Issues 7-8, June 2004, pp. 785-796. W.-K. Chen, *Linear Networks and Systems* (Book style). Belmont, CA: Wadsworth, 1993, pp. 123–135.

[2] F. Caiazzo, F. Curcio, G. Daurelio and F. Memola Capece Minutolo, Ti6Al4V sheets lap and butt joints carried out by CO_2 laser: mechanical and morphological characterization, J. of Materials Processing Technology, Vol. 149, Issues 1-3, June 2004, pp. 546-552.

[3] Z. Li and G. Fontana, Autogenous laser welding of stainless steel to free-cutting steel for the manufacture of hydraulic valves, J.of Materials Processing Technology, Vol. 74, Issues 1-3, Feb. 1998, pp. 174-182.

[4] Z. L. Zhang, J. Ødegård, O. R. Myhr and H. Fjaer, From microstructure to deformation and fracture behaviour of aluminium welded joints – a holistic modelling approach, J. of Computational Materials Science, Vol. 21, Issue 3, July 2001, pp. 429-435.

[5] W. Zhang, J. W. Elmer and T. DebRoy, Modeling and real time mapping of phases during GTA welding of 1005 steel, J. of Materials Science and Engineering A, Vol. 333, Issues 1-2, August 2002, pp. 320335.

[6] W. Zhang, T. DebRoy, T.A. Palmer and J.W. Elmer, Modeling of ferrite formation in a duplex stainless steel weld considering non-uniform starting microstructure, J. of Acta Materialia, Vol. 53, Issue 16, September 2005, pp. 4441-4453.

[7] E. M. Anawa, A. G. Olabi and F. A. Elshukri "Modeling and optimization of tensile shear strength of Titanium/ Aluminum dissimilar welded component" J. of Physics: Conference Series 181 (2009), doi:10.1088/1742-6596/181/1/012033.

[8] F. Karimzadeh, A. Ebnonnasir and A. Foroughi, Artificial neural network modelling for evaluating of epitaxial growth of Ti6Al4V weldment, J. of Materials Science and Engineering: A, Vol. 432, Issues 1-2, Sep.2006, pp. 184-190.

[9] N. Kamp, A. Sullivan, R. Tomasi and J.D. Robson, Modeling of heterogeneous precipitate distribution evolution during friction stir welding process, J. of Acta Materialia, Vol. 54, Issue 8, May 2006, pp. 2003-2014.

[10] N. Kamp, A. Sullivan and J.D. Robson, Modelling of friction stir welding of 7xxx aluminium alloys, J. of Materials Science and